Influence of the Heating Rate on the Annealing Treatment of Iron Oxide Nanostructures Obtained by Electrochemical Anodization under Hydrodynamic Conditions

Bianca Lucas-Granados, Rita Sánchez-Tovar, Ramón M. Fernández-Domene, José García-Antón*

Grupo de Ingeniería Electroquímica y Corrosión (IEC). Instituto Universitario de Seguridad Industrial, Radiofísica y Medioambiental (ISIRYM). Universitat Politècnica de València. Valencia. Spain.
jgarciaa@iqn.upv.es

Iron oxide nanostructures are promising materials for photoelectrochemical applications such as water splitting. In this work, electrochemical anodization of iron is used to form different iron oxide nanostructures, and the influence of different anodization parameters was studied in order to find the most suitable nanostructure for photocatalysis applications. On the one hand, hydrodynamic conditions were evaluated by stirring the electrode at different rotation speeds during the electrochemical anodization to check their influence on the formation of the nanostructures. On the other hand, different heating rates during the annealing treatment were studied for obtaining efficient iron oxide nanostructures. The synthesized nanostructures were characterized by different techniques such as photocurrent density vs. potential measurements, Field Emission Scanning Electron Microscopy, Raman spectroscopy and Incident Photon-to-electron Conversion Efficiency (IPCE). The results revealed that the best heating rate during the annealing treatment is 15 ºC·min^{-1} and that the hydrodynamic conditions allow the formation of nanotubular iron oxide structures achieving ~0.1 mA·cm^{-2} at 0.5 V (vs. Ag/AgCl) in the water splitting measurements. Moreover, all the nanostructures are mainly composed by hematite (α-Fe$_2$O$_3$) with some amount of magnetite (Fe$_3$O$_4$) in their structure. Finally, the IPCE measurements showed that the best rotation speed during the electrochemical anodization for the formation of an efficient iron oxide nanostructure for photocatalysis applications is 1,000 rpm.

1. Introduction

Since 1972 when Fujishima and Honda reported the use of TiO$_2$ as photoanode for photoelectrolysis of water, significantly work has been focused on developing new materials that could carry out the water splitting reaction (Fujishima and Honda, 1972). Iron is the fourth most common element in the Earth's crust and it is environmentally friendly and a low cost material (Sivula et al., 2011). Because of that, iron is an interesting element to be studied as a suitable photocatalyst for applications such as water splitting, in particular, in its nanostructured form. This is one of the reasons why nanotechnology is becoming popular in recent times (Bavasso et al., 2016).

There are different techniques that can be used to synthesize nanostructures: electrodeposition (Sunseri et al., 2016), electrochemical anodization (Ampudia et al., 2016, Lucas-Granados et al., 2016), thermal annealing (Vincent et al., 2012), sol-gel method (Qiu et al., 2007), and so on. Among them, electrochemical anodization is one of the best techniques because of the high control of its parameters (Kulkarni et al., 2016). This control is important as it determines the properties of the formed nanostructures, e.g. thickness of the layer, diameter of the nanotubes, length of the tubes, etc. Some works studied the influence of stirring the electrolyte with a magnet at a determined speed during the electrochemical anodization in order to homogenize the electrolyte and improve the formation of the nanostructures (Sarma et al., 2015). However, an interesting way to carry out the electrochemical anodization, recently investigated, is by stirring the anode (iron) using a Rotating Disk Electrode (RDE). In this way, the formation of some vortex over the anode is

avoided, and consequently, the surface of the electrode is stirred and anodized homogeneously. These hydrodynamic conditions enhance the synthesized nanostructures for photoelectrochemical applications by changing significantly their morphology. Another important parameter that controls the crystalline structure of the nanostructures is the heating rate during the annealing treatment. It is important to provide an adequate heating rate for the annealing treatment of the nanostructure in order to avoid its breakdown.

In this work, different heating rates are tested in order to form a beneficial crystalline structure for the nanostructures and, furthermore, different hydrodynamic conditions are studied for obtaining nanostructures that are efficient in the photocatalysis field.

2. Experimental procedure

Electrochemical anodization was carried out at 50 V for 15 minutes in an ethylene glycol based solution containing 0.1 M of ammonium fluoride and 3% vol. of water. Before anodization, the samples were abraded until a mirror finish was obtained (using SiC papers from 220 to 4,000) and then, sonicated in ethanol for 2 min. After that, the samples were rinsed with distilled water and dried with a nitrogen stream and then, they were ready for anodization. The electrochemical anodization configuration consisted of a cathode (a platinum foil) and an anode (iron rod 99.9 % purity) connected to a rotating disk electrode that applies different rotation speeds to the electrode during the electrochemical anodization. Once the samples were anodized, an annealing treatment was required in order to crystallize the structure to make the samples suitable for photocatalytic applications. The annealing was performed at 500 ºC for 1 hour in an argon atmosphere, and different heating rates were studied (2, 5 and 15 ºC·min^{-1}) for the different nanostructures (15 ºC·min^{-1} was the maximum heating rate that can be controlled by the used oven). The samples were cooled in the oven by natural convection.

The structural characterization was performed by using a Raman Confocal Laser Microscope (neon laser 632 nm) with ~700 μW and the morphological characterization by using Field Emission Scanning Electron Microscopy (FE-SEM). The photocurrent density versus potential measurements (water splitting tests) were carried out in a 1 M KOH solution with a solar simulator 1.5 AM (100 mW·cm^{-2}) and by scanning the potential from 0 to 0.6 V (vs. Ag/AgCl) with a scan rate of 2 mV·s^{-1}. A three-electrode configuration was used, where the counter electrode was a platinum tip, the reference electrode was a Ag/AgCl electrode (3 M KCl) and the working electrode was the studied nanostructure. The measurements were recorded by chopped light irradiation (0.02 V in the dark and 0.02 V in the light).

The Incident Photon-to-electron Conversion Efficiency (IPCE) measurements were performed in 1 M KOH under an applied potential of 0.35 V (vs. Ag/AgCl) and in the wavelength region of 300 to 600 nm. The aim of these measurements was to determine the photoactive wavelength region of the iron oxide nanostructures, and the IPCE values were calculated according to Eq. 1 (Zhang et al., 2010):

$$IPCE = \frac{1,240 \cdot i_{ph}}{P \cdot \lambda} \cdot 100$$
(Eq.1)

where i_{ph} is the photocurrent density expressed in A·cm^{-2}, P is the light power density in W·cm^{-2} and λ is the wavelength in nm.

3. Results and discussion

3.1 Water splitting measurements

Figure 1 shows the water splitting results for the samples anodized under stagnant (0 rpm) and hydrodynamic (3,000 rpm) conditions and at the different studied heating rates. It can be seen that for the samples annealed at 2 and 5 ºC·min^{-1}, the achieved photocurrent densities are significantly lower in comparison to the ones achieved for the samples anodized at 15 ºC·min^{-1}. In fact, for 2 ºC·min^{-1} and applying low potentials the current densities for the nanostructures synthesized under stagnant conditions are higher than the ones synthesized under hydrodynamic conditions but they become similar at higher potentials when the current densities are higher (and sufficient for promoting charge separation). For 5 ºC·min^{-1} and at higher applied potentials the hydrodynamic conditions increase the current densities as the potential values are enough for promoting charge separation. However, at 15 ºC·min^{-1} the current densities are higher than the ones achieved for the other heating rates at all the applied potentials for both stagnant and hydrodynamic conditions. Because of that, it seems that the most adequate heating rate in the studied range for the iron oxide nanostructure is 15 ºC·min^{-1}. Furthermore, Figure 1 c) indicates that at 3,000 rpm the photocurrent densities achieved are higher than in the case of 0 rpm, which implies that hydrodynamic conditions favour the photocatalytic performance of the nanostructures. In fact, the photocurrent density recorded at 0.5 V (vs. Ag/AgCl) for the nanostructure

anodized at 0 rpm is ~0.08 mA·cm^{-2} whereas the value for the nanostructure anodized at 3,000 rpm is ~0.1 mA·cm^{-2}, which indicates the better photoactivity of the samples anodized under hydrodynamic conditions.
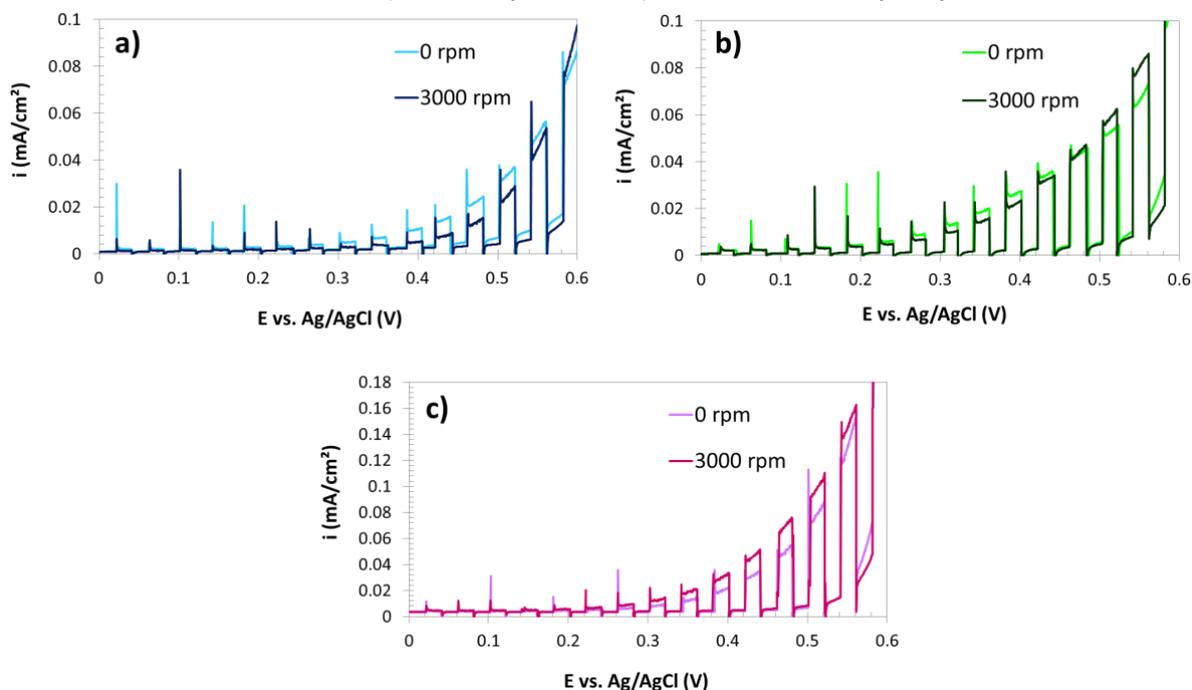

Figure 1: Photocurrent density versus potential measurements for the samples anodized at 0 and 3,000 rpm and annealed at a heating rate of 2 (a), 5 (b) and 15 ºC·min^{-1}(c).

3.2 Field Emission Scanning Electron Microscopy

Figure 2 shows the different morphologies obtained for the nanostructures synthesized at 0 (Figure 2a) and at 3,000 rpm (Figure 2b), which are both nanotubular. According to Figure 2a, the nanostructures synthesized under stagnant conditions present an initiation layer over the nanotubes which covers the entrance of the real tubes. Then, the light cannot easily arrive to the tubes to generate the electron-hole pairs that are the responsible of the photo-activity of the nanostructures. However, when the nanostructures are synthesized at 3,000 rpm (Figure 2 b)), this initiation layer partially disappears leaving the entrances of the real tubes free for favourable light illumination. The tubes that are accessible to the light are a little bit collapsed and stacked, but this is better than the initiation layer that appeared under stagnant conditions.
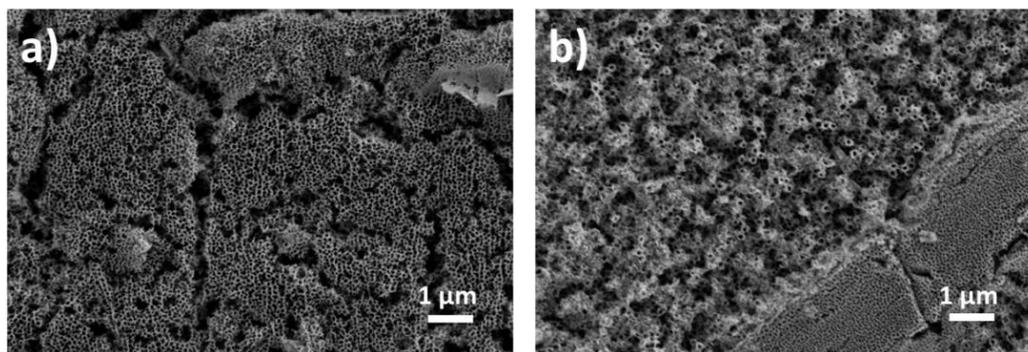

Figure 2: Field Emission Scanning Electron Microscopy images for the nanostructures synthesized at 0 rpm (a) and 3,000 rpm (b).

Hence, the hydrodynamic conditions remove part of the initiation layer that covers the entrances of the nanotubes allowing that light illuminates directly the nanotubes. This, in fact, improves the water splitting results as Figure 1 c) shows.

3.3 Raman spectra

The synthesized nanostructures are amorphous in nature, and annealing is required in order to crystallize their structure (Xie et al., 2011). This is because the defects can promote electron-hole recombination resulting in poor efficiency of the nanostructures, however when the structure is crystalline the recombination is partially avoided which enhances the nanostructures performance in photocatalytic applications. Figure 3 shows that the nanostructures synthesized at 0 and 3,000 rpm possess the same crystalline structure, which is mainly hematite (α-Fe_2O_3) with some amount of magnetite (Fe_3O_4). This is observed because the peaks of the two spectra are similar with most of the peaks corresponding to the hematite and some peaks associated with magnetite structure.
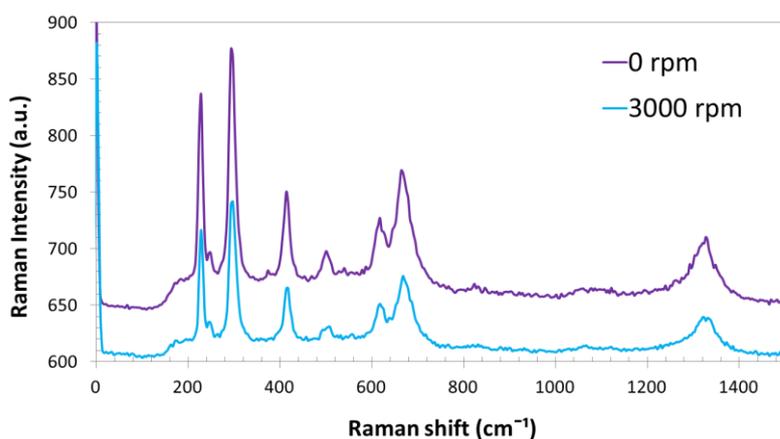

Figure 3: Raman spectra of the nanostructures anodized at 0 and 3,000 rpm

Table 1 shows the Raman shift (in cm^{-1}) of the spectra with the associated crystalline structure and the vibrational mode. Almost all the peaks are associated to the hematite structure and only three of the peaks correspond to the magnetite structure, which means that the nanostructures anodized at 0 and 3,000 rpm are mainly composed by α-Fe_2O_3 with some amount of Fe_3O_4.

Table 1: Raman peaks values for the different crystalline structures. (Jubb and Allen, 2010, Nie et al., 2013)

Raman Shift (cm^{-1})	Crystalline structure	Mode
229	α-Fe_2O_3	A_{1g}
249	α-Fe_2O_3	E_g
295	α-Fe_2O_3	E_g
414	α-Fe_2O_3	E_g
500	α-Fe_2O_3	A_{1g}
615	α-Fe_2O_3	E_g
1316	α-Fe_2O_3	2nd order
554	Fe_3O_4	T_{2g}
672	Fe_3O_4	A_{1g}

3.4 Incident Photon-to-electron Conversion Efficiency (IPCE)

The previous characterization indicated that hydrodynamic conditions favour the photocatalytic performance of the iron oxide nanostructures synthesized by electrochemical anodization. However, the tested conditions were 0 and 3,000 rpm and, since the best condition is 3,000 rpm it is interesting to check more rotation speeds of the electrode in the studied range, i.e. 1,000 and 2,000 rpm. According to this, IPCE measurements were carried out at different rotation speeds (0, 1,000, 2,000 and 3,000 rpm) with the aim of determining the best rotation speed for anodizing the nanostructures to be used as photocatalysts in IPCE measurements.
Figure 4 shows that the best photoresponse for all the studied nanostructures was in the range of 300-320 nm corresponding to the UV region. However, all the nanostructures also have some photoactivity in the visible

light region until ~450 nm. The best photoresponse was achieved for the sample anodized at 1000 rpm (~0.7 %). This fact demonstrates that the hydrodynamic conditions enhance the photoactivity of the nanostructures as was also corroborated by the water splitting measurements (Figure 1c). The IPCE results showed that the best rotation speed of the electrode during the electrochemical anodization among the studied range was 1000 rpm in order to form an efficient iron oxide nanostructure for photocatalysis.
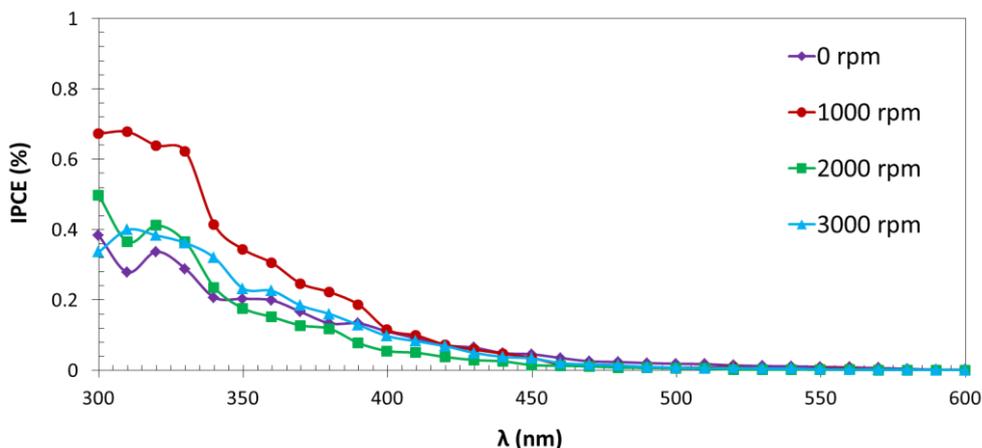

Figure 4: IPCE measurements for the samples anodized at 0, 1000, 2000 and 3000 rpm and annealed at a heating rate of 15 ºC·min^{-1}.

4. Conclusions

The water splitting results showed, on the one hand, that for the annealing process the best heating rate among the studied ones (2, 5 and 15 ºC·min^{-1}) was 15 ºC·min^{-1}, achieving the best photocurrent density values regardless the anodizing conditions. On the other hand, at this heating rate the nanostructures anodized under hydrodynamic conditions showed better results than the ones synthesized under stagnant conditions.

FE-SEM results showed that the samples anodized under stagnant conditions presented an initiation layer that covered the entrances of the nanotubes, but this initiation layer partially disappeared under hydrodynamic conditions improving the nanostructure performance in the water splitting measurements. Raman spectra showed a hematite structure with some amount of magnetite for nanostructures synthesized under stagnant and hydrodynamic conditions.

In addition, IPCE results showed that 1,000 rpm was the best rotation speed among the studied range (0 - 3,000 rpm). In summary, iron oxide nanostructures synthesized by electrochemical anodization under hydrodynamic conditions are interesting to be used as photocatalysts in photoelectrochemical water splitting.

References

Ampudia, P., Palmas, S., Vacca, A., Mascia, M., 2016, Mixed Oxides for Photo-electrochemical Applications Chemical Engineering Transactions, 47, 145–150. DOI:10.3303/CET1647025

Bavasso, I., Vilardi, G., Stoller, M., Chianese, A., Palma, L. Di, 2016, Perspectives in Nanotechnology Based Innovative Applications For The Environment, Chemical Engineering Transactions, 47, 55–60. DOI:10.3303/CET1647010

Fujishima, A., Honda, K., 1972, Electrochemical Photolysis of Water at a Semiconductor Electrode, Nat. Mater. 238, 37–38.

Jubb, A.M., Allen, H.C., 2010, Vibrational spectroscopic characterization of hematite, maghemite, and magnetite thin films produced by vapor deposition, ACS Appl. Mater. Interfaces, 2, 2804–2812. DOI:10.1021/am1004943

Kulkarni, M., Mazare, A., Schmuki, P., Iglic, A., 2016, Influence of anodization parameters on morphology of TiO$_2$ nanostructured surfaces, Adv. Mater. Lett., 7, 23–28. DOI:10.5185/amlett.2016.6156

Lucas-granados, B., Sánchez-tovar, R., Fernández-domene, R.M., García-antón, J., 2016, Formation of Hematite Nanotubes by Two-Step Electrochemical Anodization for Efficient Degradation of Organic Pollutants, Chemical Engineering Transactions, 47, 85–90. DOI:10.3303/CET1647015

Nie, S., Starodub, E., Monti, M., Siegel, D. a., Vergara, L., El Gabaly, F., Bartelt, N.C., De La Figuera, J., McCarty, K.F., 2013, Insight into magnetite's redox catalysis from observing surface morphology during oxidation, J. Am. Chem. Soc., 135, 10091–10098. DOI:10.1021/ja402599t

Qiu, J., Yu, W., Gao, X., Li, X., 2007, Fabrication and characterization of TiO$_2$ nanotube arrays having nanopores in their walls by double-template-assisted sol – gel, Nanotechnology, 18, 295604. DOI:10.1088/0957-4484/18/29/295604

Sarma, B., Jurovitzki, A.L., Ray, R.S., Smith, Y.R., Mohanty, S.K., Misra, M., 2015, Electrochemical capacitance of iron oxide nanotube (Fe-NT): effect of annealing atmospheres, Nanotechnology, 26, 265401. DOI:10.1088/0957-4484/26/26/265401

Sivula, K., Le Formal, F., Grätzel, M., 2011, Solar Water Splitting: Progress Using Hematite (α-Fe2O3) Photoelectrodes, ChemSusChem, 4, 432–449. DOI:10.1002/cssc.201000416

Sunseri, C., Cocchiara, C., Ganci, F., Moncada, A., Oliveri, R.L., Patella, B., Piazza, S., Inguanta, R., 2016, Nanostructured Electrochemical Devices for Sensing , Energy Conversion and Storage, Chemical Engineering Transactions, 47, 43–48. DOI:10.3303/CET1647008

Vincent, T., Gross, M., Dotan, H., Rothschild, A., 2012, Thermally oxidized iron oxide nanoarchitectures for hydrogen production by solar-induced water splitting, Int. J. Hydrogen Energy, 37, 8102–8109. DOI:10.1016/j.ijhydene.2011.08.088

Xie, K., Li, J., Lai, Y., Lu, W., Zhang, Z., Liu, Y., Zhou, L., Huang, H., 2011, Highly ordered iron oxide nanotube arrays as electrodes for electrochemical energy storage, Electrochem. commun., 13, 657–660. DOI:10.1016/j.elecom.2011.03.040

Zhang, Z., Hossain, M.F., Takahashi, T., 2010, Self-assembled hematite (α-Fe$_2$O$_3$) nanotube arrays for photoelectrocatalytic degradation of azo dye under simulated solar light irradiation, Appl. Catal. B Environ., 95, 423–429. DOI:10.1016/j.apcatb.2010.01.022